Batteries & Supercaps

Research Article
doi.org/10.1002/batt.202400536

Chemistry Europe
European Chemical Societies Publishing

www.batteries-supercaps.org

# Direct Recycling of $Li_xNi_{0.5}Mn_{0.3}Co_{0.2}O_2$ from Production Scrap and End-Of-Life Batteries, Using Solid-State Relithiation

Lucas Evangelista Sita,[a] Roberto Sommerville,[b] Giar Alsofi,[b] Wilgner Lima da Silva,[b] Dominika Gastol,[b] Jair Scarminio,[a] and Emma Kendrick*[b]

Direct recycling of Li-ion battery cathodes offers a sustainable and potentially cost-effective alternative to conventional methods, often involving complex chemical processes and significant material losses. This study focuses on the relithiation of cathode materials from quality control reject (QCR) and end-of-life (EoL) Li-ion cells to restore their physical structure, morphology, and electrochemical performance. Two NMC532/graphite pouch cells from the same manufacturer were studied. QCR cells, stored under ambient conditions, experienced corrosion and degradation before recycling, while EoL cells were cycled to the end of life. The cells were disassembled, and the cathode materials were delaminated using NaOH solution, then relithiated with LiOH at 700 °C for 15 hours in the air. Extensive characterization analyzed elemental composition, structural properties, thermal stability, and particle size distribution. Results indicated that relithiation successfully restored lithium content and improved the structural ordering and morphology of the cathode materials. The electrochemical performance of the relithiated cathodes exhibited good stability over 100 charge-discharge cycles. The relithiated QCR samples achieved a capacity of 155.57 mAh $g^{-1}$, while EoL samples reached 152.53 mAh $g^{-1}$, comparable to pristine materials. This study highlights relithiation's potential to extend the lifecycle of Li-ion cathodes, contributing to a more sustainable circular economy for battery materials.

## 1. Introduction

Lithium-ion batteries (LiBs) are currently the most used source of electrical energy for portable devices and electric and hybrid vehicles. Among the advantages over other battery technologies are their high energy density, long life cycle, low mass-volume ratio, and rechargeability.[1] The increasing demand for LiBs, especially in electric vehicles (EVs) and energy storage systems, has led to growing concerns regarding their environmental impact and the availability of critical materials.[1–4]

Recycling of LiBs is essential for sustainable resource management and reducing the environmental footprint of battery production.[5] Among the components of LiBs, the cathode material determines battery performance and cost-effectiveness. LiBs electrodes contain chemicals and compounds such as $LiCoO_2$ (LCO), $LiMn_2O_4$ (LMO), $LiNi_xMn_yCo_{1-x-y}O_2$ (NMC), $LiNi_xCo_yAl_{1-x-y}O_2$ (NCA), $LiFePO_4$ (LFP), graphite, lithium salts, organic binders and solvents that if improperly disposed of at the end of their service life, are harmful to the health of living beings and generate significant environmental impacts.[6] Accordingly, in the last decades, the academic and industrial community has been challenged to establish economically feasible and environmentally friendly Li-ion battery recycling processes.[7] In addition to end-of-life LIBs, production scrap cells are emerging as another source of valuable materials for recovery and recycling.[8] Production scrap can be produced at any part for the manufacturing chain; slurry, electrode or cell. These quality control rejected batteries are simpler in composition than the original packaged cells and typically have a known electrochemical material composition, as they are direct from the manufacturers and typically have not been cycled.

Large-scale LiBs recycling primarily employs hydrometallurgical and pyrometallurgical techniques or their associations with the primary objective of reclaiming valuable metals such as Li, Ni, Co, and Mn, typically achieved by transforming the cathode into pure metals or metal compounds and alloys. However, these processes in standard industrial recycling units are linked to significant greenhouse gas emissions, high energy requirements for thermal treatments, such as in the pyrometallurgy process, and the generation of substantial amounts of solvent or water waste, as seen in hydrometallurgy.[9]

In recent years, the direct recycling of cathodes (DRC) of spent LiBs has emerged as a promising alternative for the hydrometallurgical and pyrometallurgical techniques.[10] The DRC method involves the direct recovery of the cathode material from physical and chemical processes for re-use as an

[a] M. Sc. L. E. Sita, Prof. J. Scarminio0000-0003-2049-7491
Department of Physics, Londrina State University, Londrina 86057-970, PR, Brazil
Homepage: 0000-0003-2049-7491

[b] Dr. R. Sommerville, M. Sc. G. Alsofi, Dr. W. Lima da Silva, Dr. D. Gastol, Prof. E. Kendrick
School of Metallurgy and Materials, University of Birmingham, Birmingham, B15 2TT, UK
E-mail: e.kendrick@bham.ac.uk

Supporting information for this article is available on the WWW under https://doi.org/10.1002/batt.202400536

active material component. The ideal recycling route should have as few processes or steps as possible before the recycled component is re-incorporated into a cell. However, the recovered cathode materials are often lithium deficient because they have degraded in the cell during cycling or lithium has been leached in the recycling processes. Li vacancy defects in the cathode material's structure are the primary degradation mechanism of the cathode capacity loss caused by the thousands of charge-discharge cycles.[11] Other degradation mechanisms occur within cycled cathodes, including the oxidation of transition metal cations on the surface of the NMC cathode, leading to lithium loss, anti-site defects, irreversible phase transformations, and particle cracking.[10] Additionally, the reduction on Ni cations on the surface of the NMC cathode is often associated with the surface reconstruction effect, a process that transforms layered structures into spinel or rock-salt phases, contributing to further degradation.[12–15] The DRC method bypasses the need for energy-intensive and environmentally harmful processes besides minimal waste generation, preservation of valuable materials, fewer processing steps, and being environmentally friendly.[16,17]

The relithiation can be achieved through a solid-state reaction (SSR) between the cathode material and a lithium source material, such as lithium hydroxides, carbonates, or sulfates.[17] In this method, the spent cathode active material is restored to its original structure through purification methods and through repairing any structural or compositional flaws. Another important concept of the SSR method is repairing the cathode material to exhibit nearly the same electrochemical performance as the pristine cathodes.

Direct recycling routes are specific material dependent and requires the initial sorting of cells based on their cathode chemistry.[18,19] Additionally, to minimize contamination and simplify the purification step, separating the anode and cathode is preferable instead of shredding the cells, creating a mixture of anode and cathode materials.[20] Despite the need to develop strategies to reduce costs associated with manual or automatized sorting, disassembly, and non-contaminated cathode material recovering of the spent batteries, DRC offers numerous advantages over pyrometallurgical and hydrometallurgical methods, such as higher recovery rates, lower energy consumption, reduced environmental impact, and better-quality materials.[10]

The critical challenge in applying the DRC method on spent LiBs is restoring the cathode crystalline structure and composition without entirely disrupting the chemical bonds; otherwise, new non-electroactive phases can be formed.[21,22]

This work proposes a route to recycle $LiNi_xMn_yCo_{1-x-y}O_2$ cathodes of spent end-of-life (EoL) and quality control reject (QCR) pouch cells using a few-step and facile direct relithiation process. The QCR cathode was obtained from a dry cell, which had been quality control rejected before filling with electrolyte, and therefore, the dry cell stack was stored and exposed to the ambient atmosphere for several months before extraction of the cathode was attempted. This meant that the aluminium electrode was severely corroded, and where previously delamination would be simple[23] in this case, the aluminium was difficult to remove as the metal foil. Therefore, the cathode materials of these cells were extracted by dissolving the aluminum collectors in a NaOH solution and by mechanical scrapping of the cathode surfaces. The recovered powders and the relithiation products were analyzed using physical and chemical techniques such as ICP-OES, TGA-MS, FTIR, XRD and Rietveld refinement, Particle Size Analysis (PSA), and CHNS elemental analysis. Solid state relithiations of the cathode materials were carried out employing LiOH as a lithium source on reactions at 700 °C for 15 hours in an air atmosphere. The electrochemical performance of the recycled cathode was evaluated by charge-discharge cycles in a coin cell with a lithium metal anode.

## 2. Results and Discussion

Figure 1 shows the steps employed in the solid-state relithiations of the EoL and QCR cathode materials carried out at 700 °C to ensure diffusion and binding of lithium ions to the structure of these cathodes. SSR of NMC at a temperature so high as 850 °C has often been employed in the sintering step.[24]

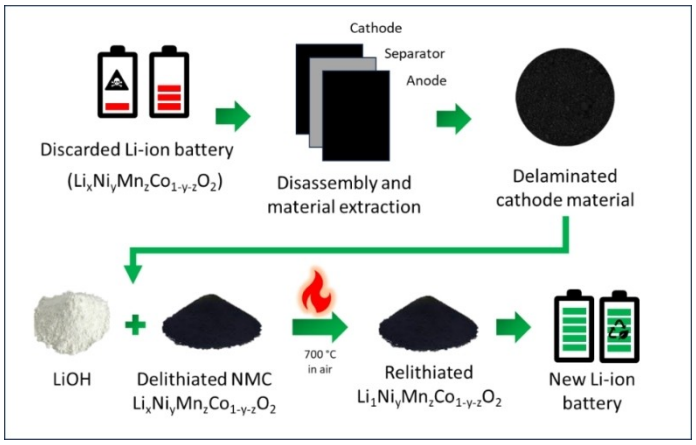


**Figure 1.** Direct recycling flow chart employed in the solid-state relithiation process.

More details about the relithiation process are depicted in the Experimental section below.

We employ air flow during the high-temperature heat treatments to ensure the replacement of oxygen eventually evolved from the cathode along the cycle-life of the cell[25] and as a reactant in the relithiation reactions to ensure the correct oxidation state of the transition metals. Thermal treatments in a non-reactive atmosphere will lead to a decomposition of the non-stoichiometric NMC cathode materials through carbothermic reactions,[26,27] as is shown by the XRD analysis in TG scan under $N_2$ atmosphere, Figure 8.

LiOH was employed as a lithium source in our solid-state reactions, as others have employed,[10,28] though other sources, such as $Li_2CO_3$, are also used.[24] Regardless of lithium sources, the SSR products aim to be the NMC stoichiometric in lithium and oxygen compositions.

Before the relithiation processes, the as-received and delaminated cathode materials were fully characterised to understand the materials' composition, structure, and potential degradation suffered by the QCR during its storage and the EoL along its useful life. These data could provide evidence for a possible correlation between the electrochemical behavior of QCR and EoL relithiated cathodes and the degradation states of the as-received and delaminated cathode materials.

### 2.1. Elemental Analysis of Cathode Materials

To determine the concentration of chemical elements in the as-received and delaminated cathode materials from QCR and EoL batteries for the subsequent relithiation process, ICP-OES analysis was performed. The results are shown in Table 1. Ni, Mn, and Co elements were identified in all samples in relative molar concentrations of 0.50:0.27:0.22, characteristic of the NMC532 cathode composition. A low aluminum concentration was also found in the powder physically removed from the surface of the as-received cathode and in the delaminated samples, indicating, therefore, a possibility that the NMC532 compound may have been doped with this element. It is known from the literature that Al as a dopant can improve thermal stability owing to the stronger strength of the Al–O bonds than those Ni, Co, and Mn–O bonds, and it also mitigates gas evolution from layered-oxides during high voltages charging.[29,30] The lithium molar concentration was equal to 1.00 for the as-received QCR cathode material, as expected for a cathode never cycled, and 0.82 for the as-received EoL cathode, showing lithium loss from formation and cycling, as is expected for end of life Li-ion batteries.

After delamination in 2.5 M NaOH solution, which selectively dissolves the aluminium current collector, the lithium concentration in the delaminated cathode material is lower than the as-received for both EoL and QCR (0.94 against 1.00 for QCR and 0.76 against 0.82 for EoL), meaning that low levels of lithium were removed from the cathode material during processing with NaOH, as shown in Table 1. ICP-OES measurements performed on the NaOH-filtered solution after the delamination process reveal the presence of lithium and no traces of Ni, Mn, Co. This is likely due to the higher rate of Li dissolution compared to Ni, Mn, Co, and Al, and the formation of lithium hydroxides on the surface, as well as its greater mobility within the NMC structure.[31] A solvent-free thermal treatment has been proposed as a delamination method that avoids the filtering step,[28] but different binder and cathode manufacturers do not guarantee the reproducibility of this process.

### 2.2. Characterization of the Cathode Materials

Figures 2 and 3 and Table 2 show data related to the structural characterization by X-ray diffraction of the as-received, delaminated, and relithiated QCR and EoL cathode materials. All diffractogram profiles correspond to the crystalline structure of $LiMO_2$ layered materials, here having Ni, Mn, and Co as the metal M in the 5:3:2 molar proportion, according to Table 1.

The as-received material showed, in addition to the presence of NMC532 compound (CIF: 242139), carbon/graphite additive (CIF: 076767), which was estimated by Rietveld refinements from its diffractograms in relative concentrations of 1.5(1) wt% and 1.2(5) wt%, for the QCR and EoL materials, respectively. In the delaminated cathode materials, the relative concentration of the carbon/graphite is lower, 0.8(1) wt% and 0.6(1) wt%, respectively, indicating some carbon of the as-received cathode materials was washed in the delamination process. In the relithiated QCR and EoL samples, only the compound $Li_1Ni_{0.50}Mn_{0.27}Co_{0.22}Al_{0.10}O_2$ (NMC532) (CIF: 242139) was identified in the XRD profile, as shown in Table 2, since conductive carbon and PVDF binder are burned at the 700 °C in the relithiation process.[32] PVDF is recognized as a low-temperature fluorination reagent for metal oxides and should therefore be avoided because it compromises the quality and integrity of the cathode material after recycling.[33,34] During calcination,

**Table 1.** Elemental analysis by ICP-OES in the NMC cathode materials of the QCR and EoL cells.

| Sample | Li | Ni | Mn | Co | Al | Stoichiometry |
|---|---|---|---|---|---|---|
| | molar ratios | | | | | |
| As-received QCR | 1.00 | 0.50 | 0.26 | 0.23 | 0.01 | $Li_{1.00}Ni_{0.50}Mn_{0.26}Co_{0.23}Al_{0.01}O_2$ |
| As-received EoL | 0.82 | 0.49 | 0.26 | 0.22 | 0.03 | $Li_{0.82}Ni_{0.49}Mn_{0.26}Co_{0.22}Al_{0.03}O_2$ |
| Delaminated QCR | 0.94 | 0.50 | 0.27 | 0.22 | 0.01 | $Li_{0.94}Ni_{0.50}Mn_{0.27}Co_{0.22}Al_{0.01}O_2$ |
| Delaminated EoL | 0.76 | 0.50 | 0.27 | 0.22 | 0.01 | $Li_{0.76}Ni_{0.50}Mn_{0.27}Co_{0.22}Al_{0.01}O_2$ |

Research Article
doi.org/10.1002/batt.202400536
Chemistry Europe
European Chemical Societies Publishing

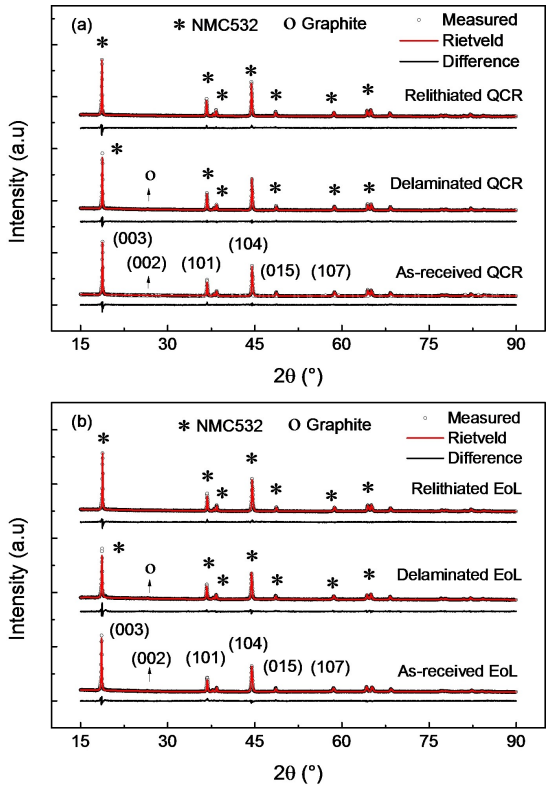


**Figure 2.** X-ray diffractograms of as-received, delaminated, and relithiated QCR (a) and EoL cathode materials (b).

reactions between fluorine compounds such as PVDF and $LiPF_6$ can lead to the formation of HF, which dopes the cathode materials by substituting oxygen and forming $MeF_2$ (Me = transition metal) or resulting in the formation of LiF on the surface.[13] XRD analysis of the relithiated materials showed no LiF or $MeF_2$ compounds, indicating minimal or no fluorination in the cathode material.

Table 2 shows the crystalline phases in the six QCR and EoL cathode materials, their relative weights, the structural evolution of *a*, *b*, and *c* lattice parameters, the *c*/*a* and $I_{003}/I_{104}$ ratios indicative of disorder degree, and the goodness of fit parameter, $\chi^2$, on the X-ray diffractograms refinements.

Besides the different lithium concentrations, the as-received and delaminated QCR and EoL cathode materials present a significant difference in their lattice parameters, particularly in the *c* and in the *c*/*a* and $I_{003}/I_{104}$ parameters, the two last as indicatives of structural order-disorder by cationic exchange.

Table 2 and Figure 3a shows that the *c* and *a* = *b* lattice parameters change their values among the as-received, delaminated, and relithiated EoL and QCR cathode materials, especially for the EoL sample. These differences are accounted for by changes in the lithium molar concentration, less or more structure disorder, and reordering by the relithiation process. The slight differences in the *c* and almost none in the *a* parameters for the QCR sample are credited to the decrease in the lithium molar concentration from 1.00 (in as-received) to 0.94 (in delaminated), followed by the reinsertion of lithium and returning concentration to 1.00 during the relithiation process. QCR material is structurally ordered with minor changes in the *c*/*a* (~4.96) and $I_{003}/I_{104} = 1.6$. On the other hand, the crystalline structure of as-received EoL cathode material exhibited lattice parameters indicative of a disordered structure characterized by lithium vacancies and significant ionic exchange. This resulted in an expanded lattice along the c-axis ($c = 14.2889(5)$ Å) and a *c*/*a* ratio of 4.99. The EoL cathode material recovered directly from the aluminium current collector by physical removing (as-received sample) showed a more ordered structure, indicating that the delamination process with NaOH solution might cause further damage to the cathode material, mainly due to lithium extraction from the NMC structure.

In the relithiated QCR and EoL samples, only the compound $Li_1Ni_{0.50}Mn_{0.27}Co_{0.22}Al_{0.10}O_2$ (NMC532) (CIF: 242139) was identified in the XRD profile, as shown in Table 2, since conductive carbon and PVDF binder, both parts of the cathode material, are burned at the 700 °C in the relithiation process.[32] Moreover, the same $a = b = 2.868$ Å, $c = 14.237$ Å lattice parameters and, $c/a = 4.96$, and $I_{003}/I_{104} = 1.6$ were measured for the QCR and EoL relithiated cathode materials, indicating no effect of the NMC532 cathode material source on the structure and ordering obtained after the relithiation.

Changes in the lattice parameters of the cathode materials are a global effect of changes in the atomic bonding lengths between Me–O and Li–O in the $MO_6$ octahedrons (Me: Ni, Mn, Co) as well as the O–Me-O and O–Li-O angles. Data presented

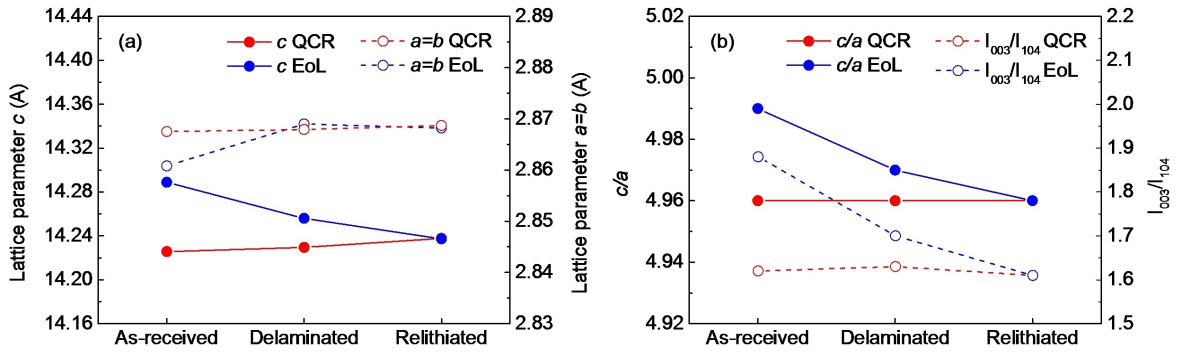


**Figure 3.** Lattice parameters *c* and *a* = *b* and (a) and c/a, $I_{001}/I_{104}$ intensity ratio for the as-received, delaminated and relithiated compounds of QCR and EoL samples (b).

Research Article
doi.org/10.1002/batt.202400536
Chemistry Europe
European Chemical Societies Publishing

**Table 2.** Crystalline phases, lattice parameters, c/a, $I_{003}/I_{104}$ and the GOF parameter for the as-received, delaminated and relithiated compounds of QC and EoL samples.

| Sample | Crystalline phases | Relative weight (%) | Lattice parameters (Å) | | | I003/I104 | $\chi^2$ |
|---|---|---|---|---|---|---|---|
| | | | a = b | c | c/a | | |
| As-received QCR | $Li_{1.00}Ni_{0.50}Mn_{0.26}Co_{0.23}Al_{0.01}O_2$ | 98.5(3) | 2.8675(1) | 14.2258(8) | 4.96 | 1.62 | 1.10 |
| | C-Graphite | 1.5(1) | 2.5122(5) | 6.710(1) | – | – | |
| As-received EoL | $Li_{0.82}Ni_{0.49}Mn_{0.26}Co_{0.22}Al_{0.03}O_2$ | 98.8(4) | 2.8608(1) | 14.2889(5) | 4.99 | 1.88 | 2.29 |
| | C-Graphite | 1.2(5) | 2.515(5) | 6.714(6) | – | – | |
| Delaminated QCR | $Li_{0.94}Ni_{0.50}Mn_{0.27}Co_{0.22}Al_{0.01}O_2$ | 99.2(4) | 2.8679(5) | 14.2295(6) | 4.96 | 1.63 | 1.67 |
| | C-Graphite | 0.8(1) | 2.29(3) | 6.720(9) | – | – | |
| Delaminated EoL | $Li_{0.76}Ni_{0.50}Mn_{0.27}Co_{0.22}Al_{0.01}O_2$ | 99.4(3) | 2.8690(1) | 14.256(1) | 4.97 | 1.70 | 1.99 |
| | C-Graphite | 0.6(1) | 2.48(7) | 6.716(5) | – | – | |
| Relithiated QCR | $Li_{1.00}Ni_{0.50}Mn_{0.27}Co_{0.22}Al_{0.01}O_2$ | 100 | 2.8687(1) | 14.2378(6) | 4.96 | 1.59 | 1.84 |
| Relithiated EoL | $Li_{1.00}Ni_{0.50}Mn_{0.27}Co_{0.22}Al_{0.01}O_2$ | 100 | 2.8682(1) | 14.2373(7) | 4.96 | 1.61 | 1.96 |

in the Supporting Information confirm a very small variation in these parameters for scrap (as-received), delaminated, and relithiated QCR cathode materials. However, these parameters change significantly among the scrapped, delaminated, and relithiated EoL cathode materials. Despite these differences, the bond lengths and angles of the QCR and EoL cathode materials converge to the same respective values after relithiations, as seen in the Supporting Information. This result is in line with the convergence for the same values of the $a = b$ and $c$ lattice and angle parameters, as described in Figure 3.

Figures 4a and b display the IR transmittance spectra for the as-received, delaminated, and relithiated EoL and QCR cathode

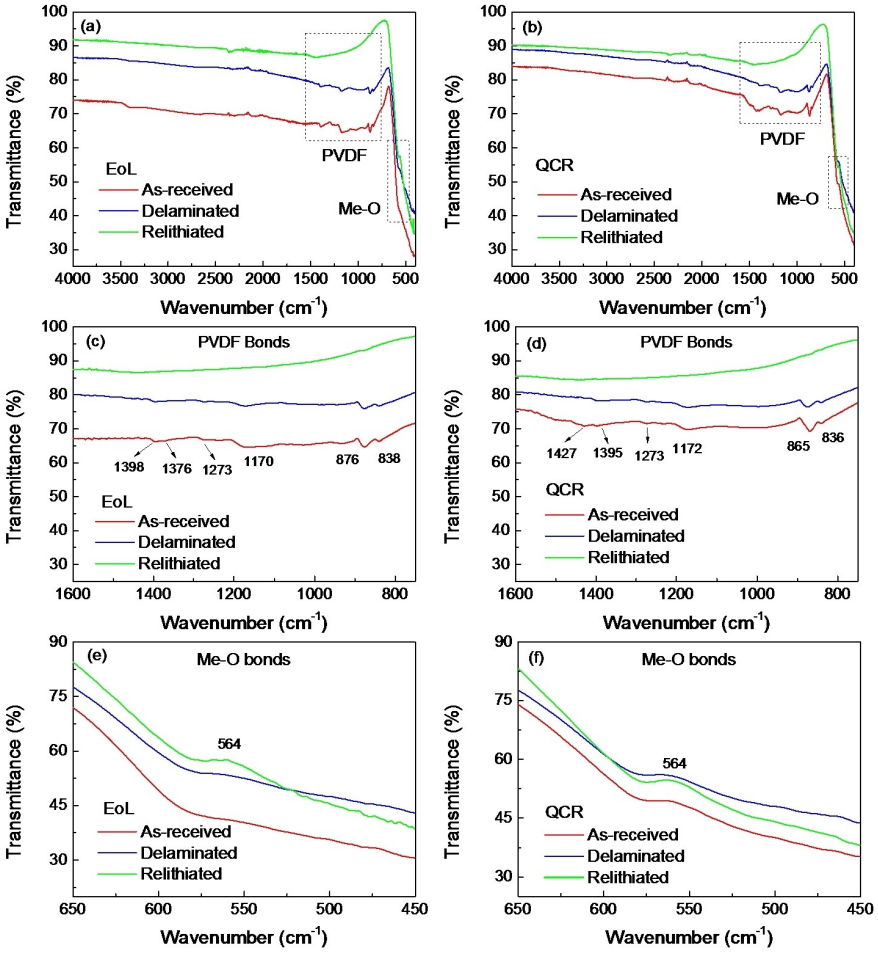


**Figure 4.** Infrared transmittance spectra for the as-received, delaminated and relithiated QCR and EoL cathode materials.

Research Article
doi.org/10.1002/batt.202400536
Chemistry Europe
European Chemical Societies Publishing

materials. Two absorption regions are of particular interest, one in the 800 to 1600 $cm^{-1}$ wavenumber range ascribed to the molecular vibrations of the PVDF binder and a second below 750 $cm^{-1}$ corresponding to Me–O bonding absorptions[35,36] in the NMC532 structure.

Six absorption peaks were identified in the 800 to 1600 $cm^{-1}$ range of the as-received EoL and QCR material IR spectra, Figures 4c and e. They are characteristic of the α, β, and γ PVDF crystalline phases. The absorption band at 838 $cm^{-1}$ belongs to the β or γ PVDF phase. Those at 876 $cm^{-1}$ and 1170 $cm^{-1}$ to the γ one, the small intensity band at 1272 $cm^{-1}$ to the β structure, and that at 1376 $cm^{-1}$ to the α form. These absorption peak intensities decrease for the delaminated samples, presumably due to reactions between PVDF and NaOH that weaken the mechanical strength and crystallinity of PVDF, even at low concentrations of NaOH, turning the PVDF structure more amorphous, leading to a decrease in the IR absorption.[37,38] The smoothness profile of the absorption curve in the PVDF absorption region of the relithiated EoL and QCR samples indicates that the PVDF binder was removed during heat treatment at 700 °C of the relithiation process.

The absorption band observed in the three NMC cathode materials at 500–600 $cm^{-1}$ range is attributed to vibration in the bonds of the $MeO_6$ octahedra, Figures 4e and f. The vibrational band around 564 $cm^{-1}$ is attributed to O–Me-O bending vibration. The IR spectra profiles of the as-received and delaminated EoL cathode material show almost no significant absorption in this wavenumber, Figure 4e, maybe due to the structural disorder typical of LiBs after many charge-discharge cycles. This argument is reinforced by the fact that a well-defined band can be seen in the absorption curve of the relithiated EoL sample, which shows a well-ordered structure, according to Table 2 data. The as-received (scraped), delaminated, and relithiated QCR samples displayed a well-defined IR absorption band at 564 $cm^{-1}$, reflecting the well-ordered crystalline structure of these samples.

Figure 4e shows that for the as-received and delaminated EoL cathode materials, the absorption bands' wavenumbers corresponding to the Me–O bonds' vibrations are lower than the 564 $cm^{-1}$ absorption wavelength for this cathode after its relithiation. In opposition, absorptions by the Me–O bonds occur at the same 564 $cm^{-1}$ for scrapped, delaminated, and relithiated QCR cathode materials, as displayed in Figure 4f, indicating the high crystal stability and atomic order of these cathode materials. Figures 4e and f display the significant result: the IR absorption from Me–O vibration in the relithiated NMC cathode material occurs at 564 $cm^{-1}$, independently of the material source.

The absorption band in the 1800 to 1900 $cm^{-1}$ range assigned to typical solvents such as EC, DMC, and DEC are absent in the FTIR curve, indicating electrolyte-free EoL and QCR cathode materials.

SEM images and EDX mapping analysis for the as-received, delaminated, and relithiated QCR and EoL cathode materials are shown in Figures 5 and 6, respectively. The images of the as-received QCR powder, Figures 5a and b, show large particles and spherical clusters surrounded by a continuous and granular material, which, according to EDX images, are small NMC particles. Figure 5b SEM images show a coating covering the surface of some large particles, which could be lithium residues, carbonates, and hydroxides, resulting from the exposure of the open battery to air for a long storage time. PVDF binder,

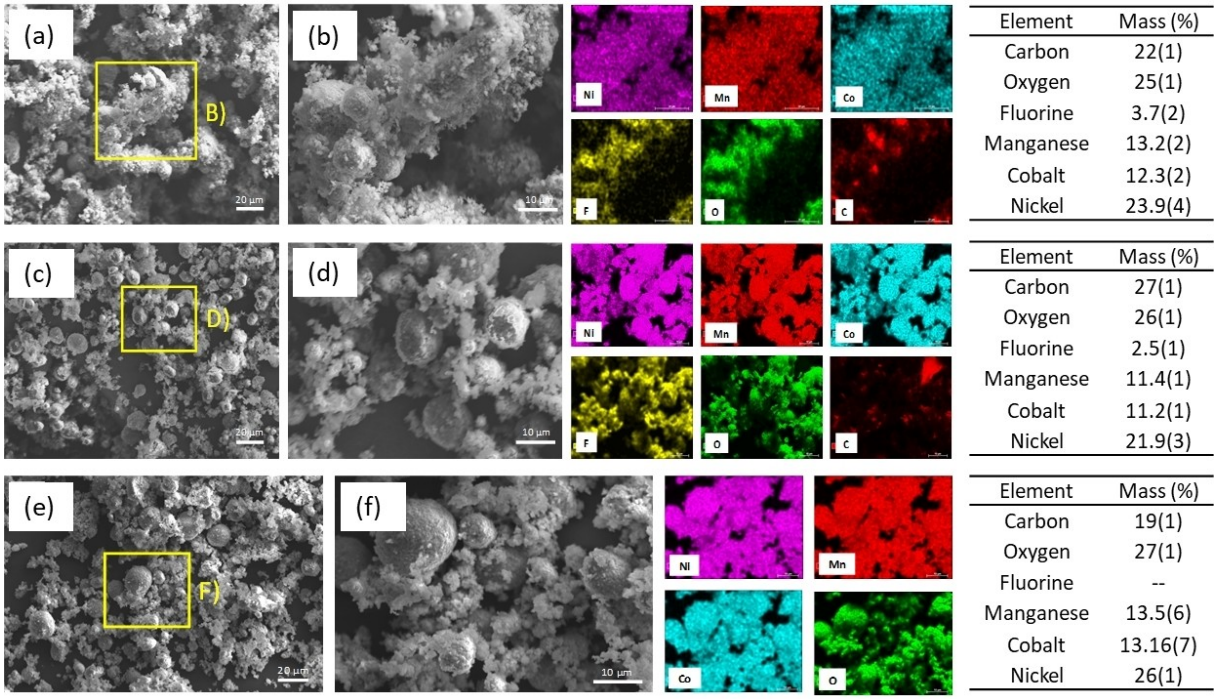


| Element | Mass (%) |
|---|---|
| Carbon | 22(1) |
| Oxygen | 25(1) |
| Fluorine | 3.7(2) |
| Manganese | 13.2(2) |
| Cobalt | 12.3(2) |
| Nickel | 23.9(4) |

| Element | Mass (%) |
|---|---|
| Carbon | 27(1) |
| Oxygen | 26(1) |
| Fluorine | 2.5(1) |
| Manganese | 11.4(1) |
| Cobalt | 11.2(1) |
| Nickel | 21.9(3) |

| Element | Mass (%) |
|---|---|
| Carbon | 19(1) |
| Oxygen | 27(1) |
| Fluorine | -- |
| Manganese | 13.5(6) |
| Cobalt | 13.16(7) |
| Nickel | 26(1) |

**Figure 5.** SEM and EDX analysis of as-received (a) and (b), delaminated (c) and (d), and relithiated (e) and (f) QCR cathode materials.

Research Article
doi.org/10.1002/batt.202400536
Chemistry Europe
European Chemical Societies Publishing

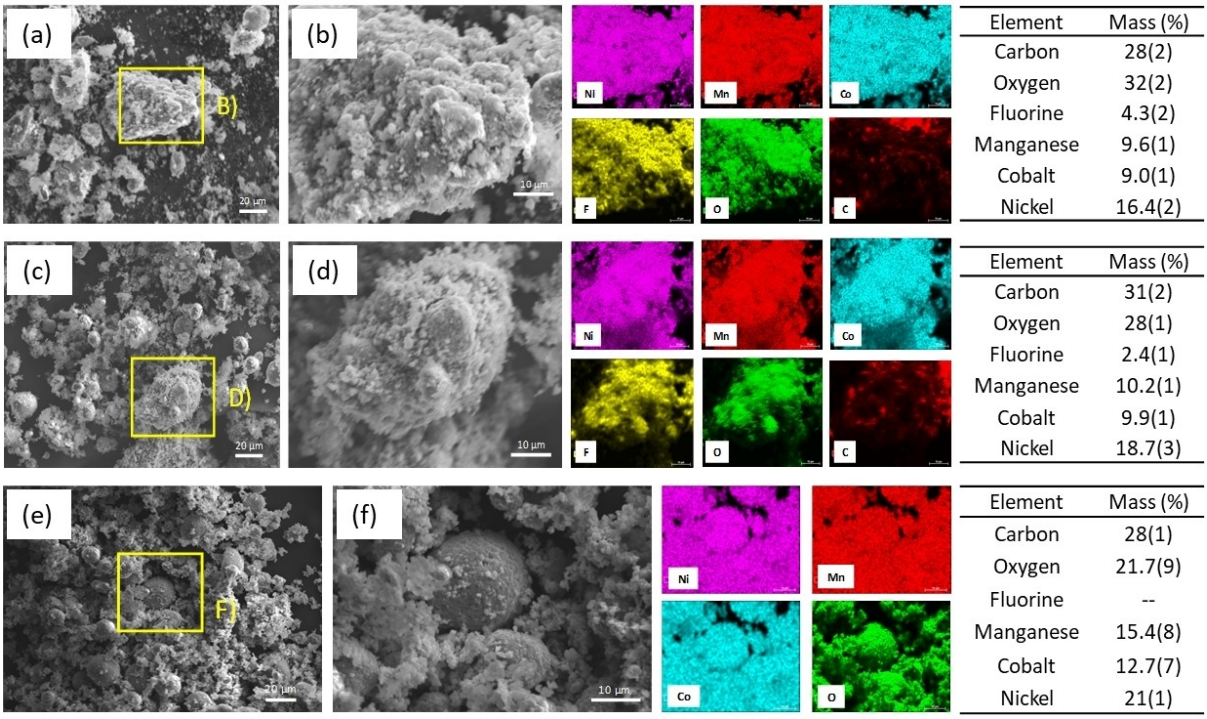


| Element | Mass (%) |
|---|---|
| Carbon | 28(2) |
| Oxygen | 32(2) |
| Fluorine | 4.3(2) |
| Manganese | 9.6(1) |
| Cobalt | 9.0(1) |
| Nickel | 16.4(2) |

| Element | Mass (%) |
|---|---|
| Carbon | 31(2) |
| Oxygen | 28(1) |
| Fluorine | 2.4(1) |
| Manganese | 10.2(1) |
| Cobalt | 9.9(1) |
| Nickel | 18.7(3) |

| Element | Mass (%) |
|---|---|
| Carbon | 28(1) |
| Oxygen | 21.7(9) |
| Fluorine | -- |
| Manganese | 15.4(8) |
| Cobalt | 12.7(7) |
| Nickel | 21(1) |

**Figure 6.** SEM and EDX analysis of as-received (a) and (b), delaminated (c) and (d), and relithiated (e) and (f) EoL cathode materials.

detected by FTIR and illustrated by fluorine in the FTIR analysis, is present between the particles. After the delamination process with NaOH solution, Figures 5c and d, occurs a deagglomeration of the particle cluster due to the reactions between PVDF and NaOH aqueous solution, as described previously, decreasing the fluorine relative weight from 3.7(2)% in the as-received QCR to 2.5(1)% in the delaminated sample, qualitatively confirmed by the decrease in the FTIR bands of the PVDF showed in Figure 4c and d. The relithiated QCR sample, Figures 5e and f, show clean and rounded grains fluorine-free, as the PVDF was eliminated during the thermal treatment at 700 °C for 15 hours. FTIR and SEM-EDX analyses confirmed the elimination of PVDF, and no LiF was identified by these techniques, which is consistent with the XRD results.

SEM images of the as-received EoL sample, Figures 6a and b, show large clusters of particles of irregular shapes. PVDF binder covers these particle surfaces according to the EDX images. The fragmentation of the grains may have occurred as an effect of charging and discharging the battery till its end of life, in which lithium ions are extracted from and inserted into the cathode particles. This process causes the particles to expand and contract, generating internal mechanical stresses.[39] Various mechanisms relieve these internal stresses, such as particle cluster disaggregation, particle cracking, progressing to particle fractures, and eventually particle disintegration.[40] The powder extracted from the EoL cathode by delamination by NaOH current collector dissolution, Figures 6c and d, led to the same behavior as observed for the QCR sample: deagglomeration and a decrease in the fluorine concentration, 4.3(2) in the as-received and 2.4(1) in delaminated, in weight %. Figures 6e and f show a change in the particle morphology of the relithiated EoL sample, presenting clean and rounded particles with regular surfaces embedded in a host of smaller networked NMC particles. No fluorine was measured for this sample by EDX analysis, indicating complete burning of the PVDF binder into gas products. Ni concentration measured by the EDX technique in all six samples is over twice that obtained for Mn and Co, following the concentration measured by ICP-OES for these elements, as displayed in Table 1.

SEM and EDX data suggest that the QCR and EoL as-received cathode materials have different degradation types that hold some morphological characteristics even after the delamination and relithiation processes, which could be reflected in their chemical and physical properties.

The carbon relative concentrations detected in all samples do not express the actual carbon content in the cathode materials since they include the carbon tape used to fix them into the EDX sample holder. Low concentrations or even no carbon is expected for the relithiated samples. To follow the actual carbon content in the cathode materials along their processing a CHNS analysis was carried out in the as-received, delaminated, and relithiated QCR and EoL samples, as shown in Table 3, also including data on hydrogen, nitrogen, and sulfur concentrations.

The main element identified in all samples was carbon, which in a cathode electrode can be present in the PVDF binder and in the graphite or carbon black conductor. In the as-received samples, carbon was found in its higher concentrations (between 4.6 and 5.2%, respectively), which slightly decreased in the delaminated QCR and EoL samples, probably due to the

Research Article
doi.org/10.1002/batt.202400536
Chemistry Europe
European Chemical Societies Publishing

**Table 3.** CHNS elemental analysis in the as-received, delaminated and relithiated QCR and EoL cathode materials.

| Sample | Carbon (wt%) | Hydrogen (wt%) | Nitrogen (wt%) | Sulfur (wt%) |
|---|---|---|---|---|
| As-received QCR | 4.62 | 0.17 | ND | ND |
| As-received EoL | 5.42 | 0.38 | ND | 0.09 |
| Delaminated QCR | 4.18 | 0.15 | ND | ND |
| Delaminated EoL | 4.30 | 0.30 | ND | ND |
| Relithiated QCR | 0.07 | 0.01 | ND | ND |
| Relithiated EoL | 0.08 | 0.01 | ND | ND |

ND = not detected.

carbon thinnest particles having passed through the fiberglass filter and gone into the solution, in the filtration of the NaOH dissolution process.

For the relithiated samples, the carbon concentration decreases drastically, approaching zero for both samples: 0.07 wt% and 0.08 wt% for the QCR and EoL samples, respectively. These results confirm that the conductive carbon and those from the binder present in the as-received samples were wholly burned after the 700 °C relithiated process, and this powder was further processed as a material free of carbon. The decrease in carbon concentration was also detected in the XRD and Rietveld refinement results, as shown in Table 2, with relative concentrations slightly different because the PVDF is amorphous.

The hydrogen element present in all samples can be attributed to the PVDF composition ($C_2$-$H_2$-$F_2$). Sulfur was obtained only for the as-received EoL sample in a minimal concentration of 0.09 wt%).

Figure 7 shows the particle size distribution (PSD) for the as-received, delaminated, and relithiated QCR and EoL samples. For the as-received cathode materials, Figures 7a and b, it is observed particles with an extensive size distribution range: 0.4 to 296.0 μm for the QCR and 0.3 to 249.0 μm for the EoL, resulting in an average particle size of 55.14 μm and 37.84 μm, respectively. The recorded highest sizes (> 200 μm) are not ascribed to single particles but agglomerates of them by the

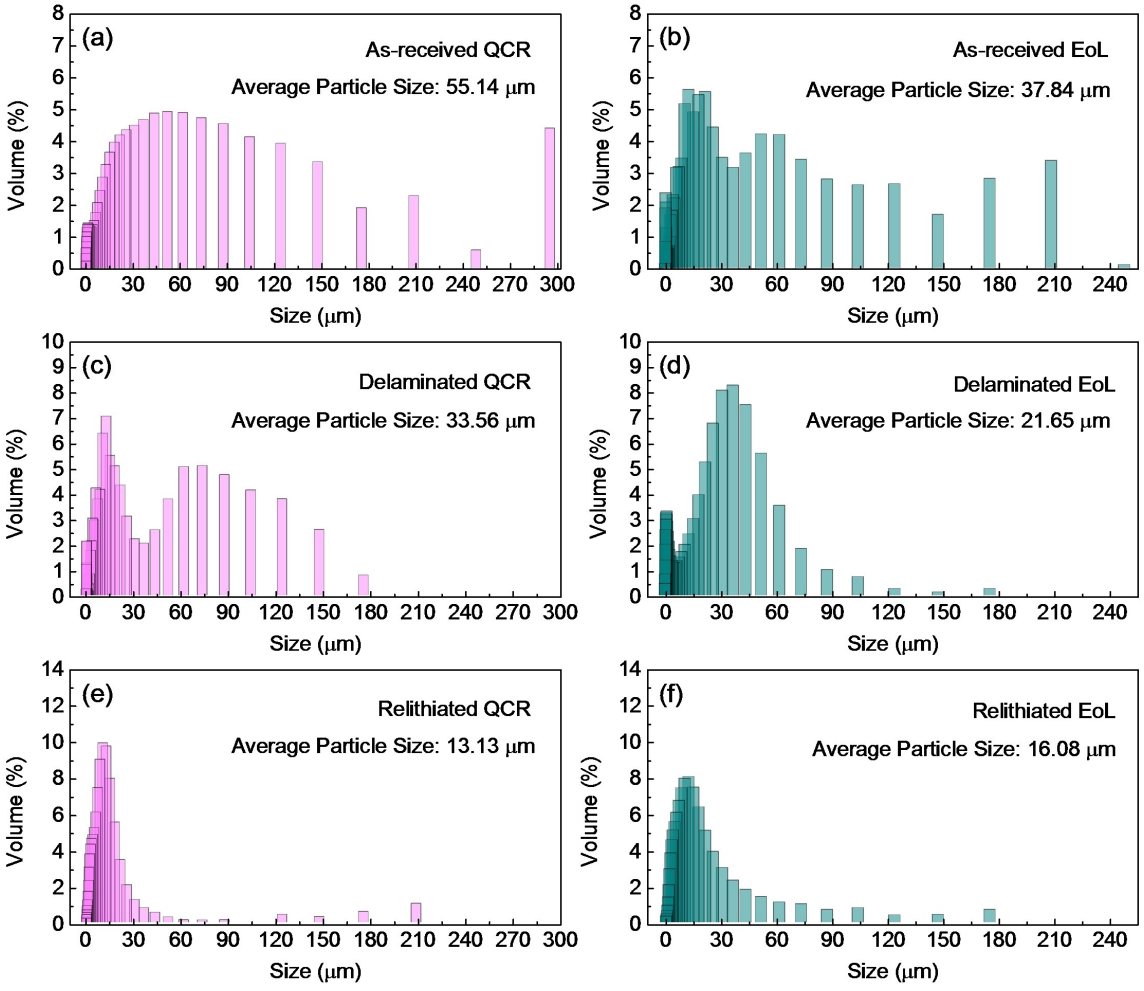


**Figure 7.** Particle size distributions of the as-received, delaminated, and relithiated EoL and QCR sample.

Research Article
doi.org/10.1002/batt.202400536
Chemistry Europe
European Chemical Societies Publishing

binder. It should be noted that the as-received samples were first macerated and sieved through 40 μm meshes before the PSA measurements.

After delamination with NaOH solution, a decrease in the size distribution range is observed for both the QCR and EoL samples: 0.4 to 176 μm and 0.3 to 176 μm, respectively. Accordingly, the average particle size distribution decreased: to 33.56 μm for the QCR and 21.65 μm for the EoL samples. This effect might have occurred due to the particle disaggregation caused by the weakening of the PVDF bonds in the NaOH solution during the delamination process. It is known from the literature that even at low concentrations of NaOH, the PVDF bonds could be partially dissolved.[37,38] This phenomenon was confirmed by FTIR analysis, as shown in Figure 4. After the relithiation process, most of the binder and additive carbon binder is burned during the thermal treatment at 700 °C (confirmed by FTIR, and CHNS elemental analysis), and a complete deagglomeration of particles occurred, exposing free particles that disclose their actual sizes. The extensive particle size distribution range for the as-received and delaminated samples was drastically shorted after the relithiation with the QCR particle sizes concentrated in the 0.3 to 90 μm range and the EoL from 0.4 to 120 μm range. Similar average particle sizes of 13.13 μm and 16.08 μm were then measured for the relithiated QCR and EoL samples, respectively.

As described, the relithiation process is carried out by calcinating the mixture of the delaminated cathode material with LiOH at 700 °C for 15 hours under airflow to achieve the NMC532 material with a lithium molar concentration equal to one. Reactions between the NMC material, PVDF binder, conductive carbon, absorbed water, and eventual electrolyte residue could occur along the calcination process.

The products resulting from the cathode material calcination are explored by TG scanning on the as-received QCR and EoL cathode materials under a nitrogen atmosphere, in which the MS technique identifies the volatile products, Figures 8a

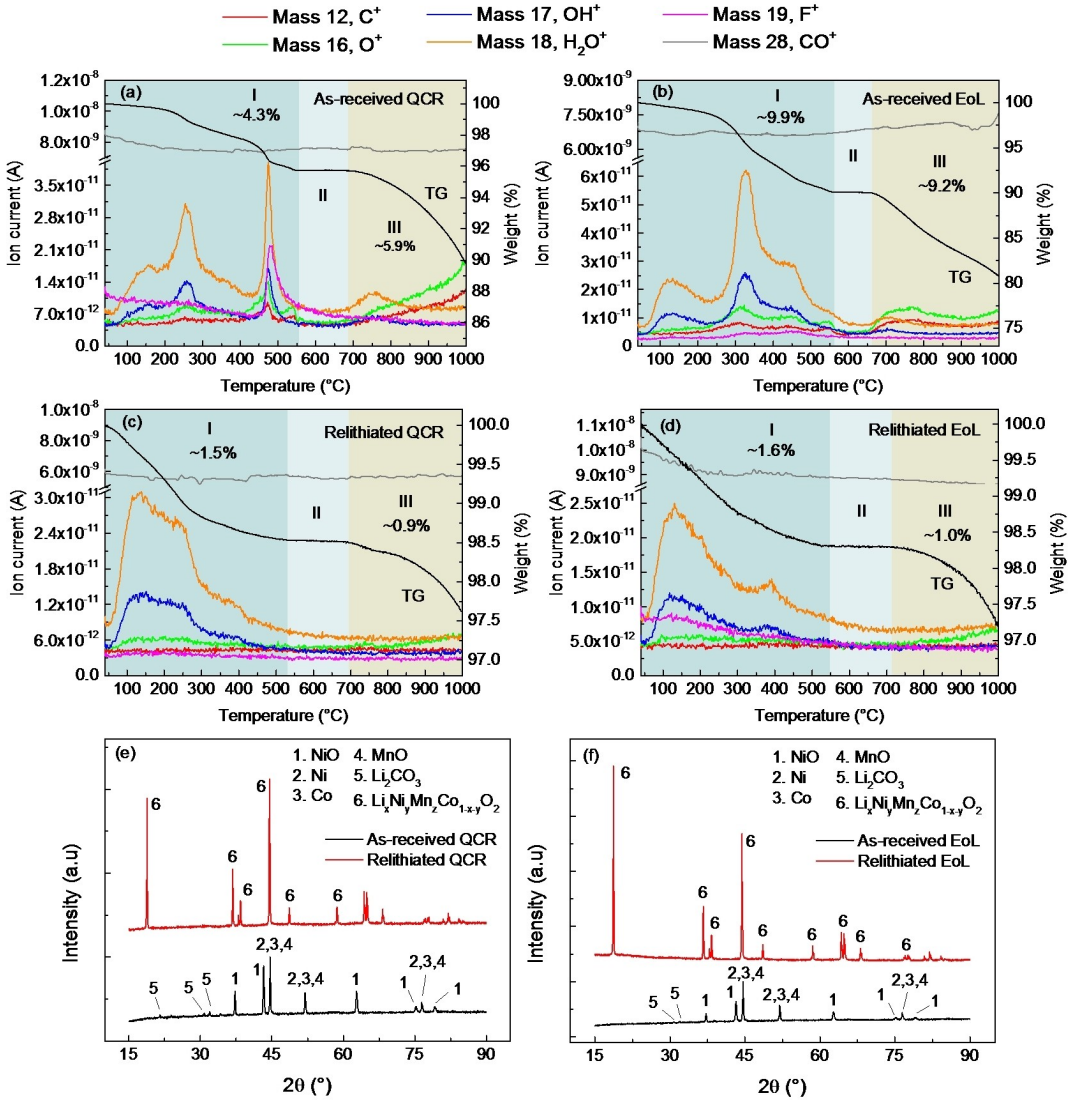


**Figure 8.** TG scanning in $N_2$ atmosphere of the As-received and relithiated EoL and QCR cathode materials with simultaneous identification of the released mass by MS (a to d) and their XRD patterns at the end of TG (e and f).

and b. The thermal stability of the relithiated material is also analised by TG and DRX measurements, Figures 8c to 8f. XRD profiles were taken at the end of TG scanning after the samples had cooled down.

Figures 8a and b show the as-received EoL and QCR samples lost around 10 and 20% of their respective masses, against less than 3% after their relithiatiations, Figures 8c and d, indicating thermal stability of the relithiated samples in $N_2$ atmosphere, in agreeing with the reported data correlating a decrease in the NMC cathodes thermal stability with the decrease in the lithium molar concentration.[41] Simultaneous MS analysis showed that the cathode mass loss is mainly due to evolved $CO_2$, water, and fluorine gases, attributed to the thermal decomposition of the carbon additive, PVDF binder, and eventual residual electrolyte.[28,41,42]

Figures 8e and f show the X-ray diffractograms of the products formed at the end of the TG scanning (1000 °C) for the as-received EoL and QCR cathode materials. Besides the volatiles described in Figures 8a and b, five other solid products, $Li_2CO_3$, NiO, Ni, MnO, and Co were identified in the X-ray diffraction patterns after the calcination of the QCR and EoL scrapped cathode materials as displayed at the bottom of Figures 8e and f, indicating that the As-received non-stoichiometric (in lithium) cathode materials are not thermally stable and are fully decomposed along the TG scanning. These compounds and metals are well-known products of carbothermic reactions between the NMC and carbon, which is present in cathode materials as conductor graphite and the binder.[43–45] Carbothermic reactions can also occur when the cells are shredded and thermal runaway happens.[46] In both scenarios, these reactions result in a highly contaminated black mass that cannot be directly recycled. This should be taken into account when considering scalable processes for direct cathode material recycling.

Conversely, only the NMC compound was identified from the X-ray diffraction patterns of the relithiated EoL and QCR samples, shown at the top of Figures 8e and f, indicating that the hexagonal structure of the stoichiometric relithiated samples does not decompose even after being heat treated till 1000 °C in $N_2$ atmosphere, confirming any carbon impurities were removed in the relithiation stage. The $I_{003}/I_{004}$ ratio displaced from the 1.2 ideal value for a well-ordered structure indicates that some disorder was introduced in the hexagonal structure of the two relithiated samples at the end of the TG scan.

### 2.3. Electrochemical Performance

After confirming the relithiation process and impurities removal, electrochemical performances were evaluated via half-cell configuration as described in the experimental section. Figure 9 presents the voltage profiles obtained in the electrochemical formation process and cycling of the electrodes mounted with the EoL and QCR relithiated cathode materials and with the original cathodes, which did not undergo any treatment. The cells' performances with the original and relithiated cathode materials were compared to each other in two formation cycles.

The original QCR cathode is relatively stable after two cycles, but after charging 170 mAh g$^{-1}$, the cell hits the 4.3 V limit, followed by a short constant voltage step and then an ohmic drop to 4.2 V, Figure 9a. No stability was found for the original EoL cathode after two charge-discharge cycles, which after 82 mAh g$^{-1}$ hit the 4.3 V limit and dropped to 4.0 V after the end of the CV charging step, Figure 9b. The impedance in the original QCR and EoL cathodes answers these electrochemical behaviors, with overpotentials of the EoL cathode higher than the QCR one.

On the other hand, two cycles were enough to stabilize the fresh relithiated QCR and EoL cathodes in the test cell under a current of 10 mA g$^{-1}$, at the expense of charge loss around 23 mAh g$^{-1}$, from the first to the second cycle, Figures 9c and d. Charge capacities (at the discharges) around 159.0 mAh g$^{-1}$ were obtained at the end of the second cycle for relithiated QCR and EoL cathodes. The lower efficiency of the first cycle expresses the loss of 23 mAh g$^{-1}$ between the charge inserted in the charging step and that delivered in the discharging in reactions to form the SEI layer on the anode carbon particles.[47–49]

The superimposition of three voltage curves during the charging and the two discharging curves in the 10$^{th}$, 50$^{th}$ all under a current of 30 mA g$^{-1}$, emphasize the high electrochemical stability of the relithiated QCR cathode after one hundred charge and discharge cycles, Figure 9e. The high discharge current of 150 mA g$^{-1}$ (after the charging at 30 mA g$^{-1}$) accounts for the displacement of the discharge curve to lower voltages. The displacement between the 10th and 50th discharge curves shown in Figure 9f reveals that the relithiated EoL cathode is less electrochemically stable than the relithiated QCR, with a progressive loss of charge along the charge-discharge cycles. Although the charge lost from the 10$^{th}$ to 50$^{th}$ cycle was small (5.6 mAh g$^{-1}$), this is an unexpected effect from the structural point of view since the relithiated EoL cathode material presented the same lattice parameters as the relithiated QCR one, and Table 2 data indicates none or very low cationic exchange.

Figure 10 illustrates the specific discharge capacity dependence of the relithiated QCR and EoL electrodes with the number of charge-discharge cycles, employing 30 mA g$^{-1}$ in the charge step and 30 mA g$^{-1}$ or 150 mA g$^{-1}$ in the discharge one. The cell with the relithiated QCR cathode initially had a capacity of 155.57 mAh g$^{-1}$, which decreased to 152.75 mAh g$^{-1}$ after one hundred cycles. Similarly, the cell of the relithiated EoL showed an initial capacity of 152.53 mAh g$^{-1}$, which decreased to 142.98 mAh g$^{-1}$ at the end of the hundredth cycle, reflecting the lowest electrochemical stability of this cathode, as mentioned above. Considering that all cells have the same configuration except for the cathode material, the decrease in charge capacity observed in the EoL cell with cycling likely stems from the different electrochemical properties of the relithiated EoL and QCR cathodes. As observed from the SEM images (Figure 6), some large agglomerated particles from EoL have been broken or cracked during the processing. The faster

Research Article
doi.org/10.1002/batt.202400536
Chemistry Europe
European Chemical Societies Publishing

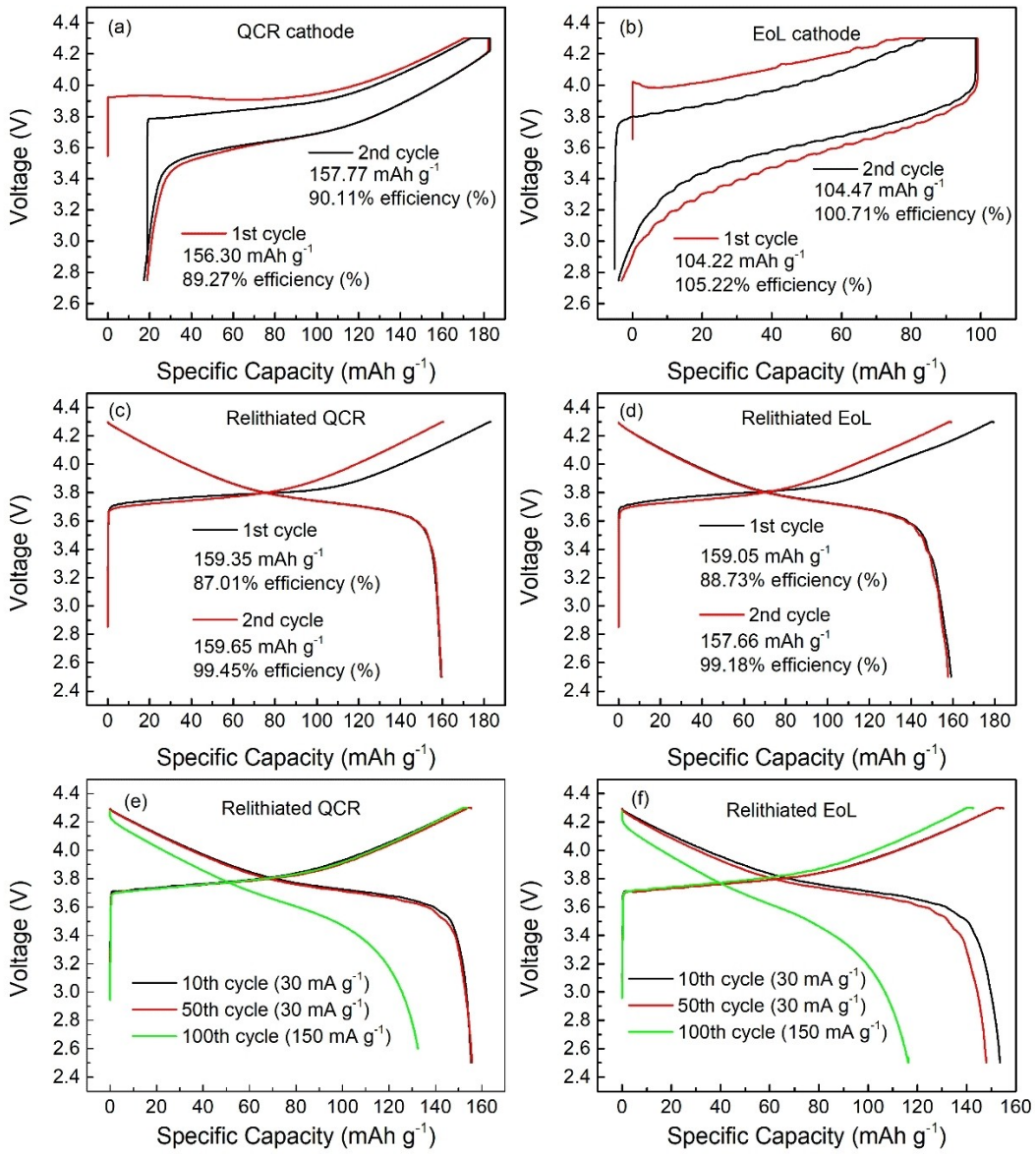


**Figure 9.** Formation charge-discharge cycles for the original QCR and EOL cathodes (a) and (b), respectively, and for their relithiated cathode (c) and (d). The 10th, 50th, and 100th charge-discharge cycles for the relithiated QCR and EOL cathodes are presented in (e) and (f).

capacity fade rate with the re-lithiated EOL cathode is likely due to the higher surface area of the active material particles, and increased degradation occurring during cycling. However, further data is needed for a better understanding of this effect. It is expected that to optimise further direct recycling routes, particle morphology and re-engineering of the materials must be considered, not just the crystal structure. This is the subject of future work. However, the obtained charge capacities are aligned or even better than those reported in the literature. As a few examples, solid-state relithiation of NMC532 and NMC111 with $Li_2CO_3$ at 850 °C in $O_2$ atmosphere for 4 h resulted in electrodes with 125 mAh $g^{-1}$ capacity after 100 cycles (3.0–4.5 V) at 0.1 C rate; electrodes of discarded NMC532 cathode relithiated under a $LiNO_3$-LiOH eutectic solution followed by heat treatment at 850 °C for 4 h delivered 135 mAh $g^{-1}$ after 100 cycles (3.0–4.3 V) in 0.1 C rate; capacity of 133 mAh $g^{-1}$ after 100 cycles (2.5–4.3 V) at 0.2 C was obtained for electrode manufactured from relithiation of spent NMC111 carried out with $Li_2CO_3$ ball milling and 800 °C sintering two steps process.[24] The capacity of 146 mAh $g^{-1}$ in 0.33 C (3.0–4.3 V) was reported after 50 cycles of charge-discharge of electrodes manufactured from relithiated NMC111 with $LiOH.H_2O$ solid state reaction at 350 °C for 4 h followed by a 4 h annealing at 650 °C.[21] Furthermore, an excellent charge capacity recovery was observed when the cell, after being discharged at 150 mA $g^{-1}$ returned to charge-discharge cycles upon 30 mA $g^{-1}$ of current density.

The Coulombic efficiency is kept at 100% along the one hundred charge-discharge cycles performed at 30 mA $g^{-1}$ of current density but decayed to values around 80–90% when discharged at 150 mA $g^{-1}$, as expected from cells discharged at rates higher than the charging rates as an effect of ohmic loss and concentration polarizations. A Coulombic efficiency higher

Research Article
doi.org/10.1002/batt.202400536
Chemistry Europe
European Chemical Societies Publishing

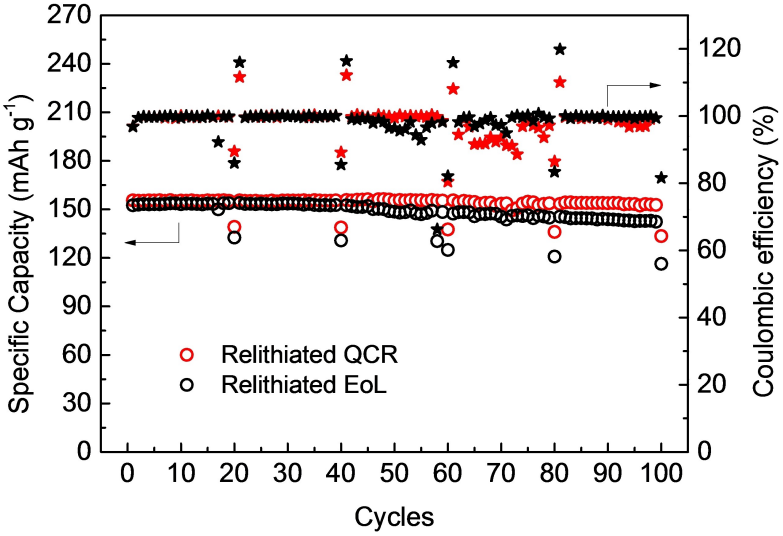


**Figure 10.** Specific discharge capacity as a function of the number of charge-discharge cycles.

than 100% was measured in the charge-discharge cycles carried out at 30.0 mA $g^{-1}$ just after the discharge on 150 mA $g^{-1}$ as an effect of the residual charge remaining in the cathode under this discharge for the relithiated QCR and EoL cathodes and its Coulombic efficiency

## 3. Conclusions

The literature on direct relithiation (DR) techniques for cathodes of LIBs from production scrap and about methods for extracting the cathode material without using shredding and/or pyrometallurgical steps is limited. This study explores the application of DR techniques to two types of cathodes: one for non-stoichiometric and structurally defective from an end-of-life (EoL) pouch cell, and the other for stoichiometric and well-ordered from a quality control reject (QCR) pouch cell. Extracting the QCR cathode material from a dry cell exposed to the atmosphere for several months proved challenging due to severe aluminum corrosion. Extensive analyses were necessary to understand the as-extracted cathode material from the rejected cell until the relithiation process. The delamination step by the dissolution of the aluminum collector decreases the lithium concentration in both cathodes, which should be accounted for in the lithium concentration adjustment. The DR by solid-state reaction with LiOH at 700 °C under air atmosphere applied to both delaminated cathode materials resulted in NMC532 compounds: a) stoichiometric ($Li_1Ni_{0.5}Mn_{0.3}Co_{0.2}O_2$) and highly ordered, b) free of organic impurities (PVDF and carbon), c) formed by large spherical particles surrounded by a network of small ones, with the network of smaller particles being predominant in the morphology of the relithiated EoL material. Cells built with the relithiathed cathodes showed a starting charge capacity of 155.57 mAh $g^{-1}$ with a low charge lost with cycling. At the end of a hundred charge-discharge cycles, the capacity losses were 2.82 and 9.55 mAh $g^{-1}$ for the relithiated QCR and EoL cathodes, respectively, reflecting lower electrochemical stability for the EoL cathode. Since XRD measurements indicate that the relithiation of QCR and EoL cathodes results in stoichiometric materials with the same structure and order but with slightly different morphologies, it can be argued whether this parameter is influencing the electrochemical stability of the electrodes.

## Experimental

### QCR and EoL Discarded Cells

In this study, two $Li_xNi_yMn_zCo_{1-y-z}O_2$ (NMC)/graphite pouch cells from the same manufacturer and model were used, one picked up from a quality control reject dry cells (QCR) and the other from end-of-life (EoL) cells. QCRs are defective cells discarded by the manufacturer without electrolytes and have never been cycled. They were received open on one bag side and stored in the ambient atmosphere for several years, causing corrosion of the Al current collectors. On the other hand, EoL cells are operational cells cycled until exhaustion. The cells were manually opened, giving access to the electrodes and separator, which were carefully withdrawn, resulting in isolated sheets of the cathode, anode, and separator.

After disassembling the end-of-life (EoL) entire cell (including cathode, anode, separator, lithium salt, and organic solvents), the cathode was soaked in isopropyl alcohol (IPA) for 1–2 hours. This step aimed to dissolve the ethylene carbonate (EC) and diethyl carbonate (DEC) from the electrolyte. Subsequently, the cathodes were dried in a hot vacuum to remove and evaporate any remaining solvent residues.

### Cathode Delamination and Relithiation Processes

The cathode material was delaminated from its aluminum collector using a 3.5 mol $L^{-1}$ NaOH solution to dissolve the Al foil selectively. Cut pieces of the cathode sheets were immersed into the NaOH solution at 70 °C for 1 hour under magnetic stirring. After the

dissolution procedures, the solution was vacuum filtered using a glass membrane filter to separate the undissolved reaction products, which were dried at 60 °C for 24 hours.

Cathode materials were also extracted by manually scraping the cathode surfaces before proceeding to the delamination process. From now on, these samples will be named QCR or EoL as-received samples. The cathode materials obtained by delamination and removal were macerated in a mortar and sieved through a 40 mesh.

The solid-state relithiation of the delaminated NMC cathode materials extracted from the QCR and EoL cells was carried out in a tubular furnace with LiOH as a lithium source. The relative weight of the cathode material and LiOH differs in the mixture of the powders for the EoL and QCR samples due to their distinct lithium concentrations. Specifically, for every gram of as-received EoL cathode material, 0.0738 g of LiOH was carefully weighed for the mixture. Conversely, a different ratio was applied for each gram of as-received QCR cathode material, with 0.0271 g of LiOH used. Each mixture was processed in a ball mill at 300 rpm for 20 minutes, followed by calcination at 700 °C for 15 hours under airflow. These ratios between the as-received NMC and LiOH materials correspond to a molar proportion of lithium to metal of 1.05 : 1.

### Cathode Material Characterizations

Inductively coupled plasma optical emission spectroscopy (ICP-OES-Agilent 5110) identified the chemical elements in the as-received and delaminated cathode materials extracted from both cells.

Infrared spectra recorded with an FTIR iS50 (Thermo Scientific) spectrometer in transmission mode from 400 to 4000 wavelengths $cm^{-}1$ range were employed to identify the chemical compounds of as-received and delaminated samples and after their solid-state relithiation.

A Panalytical X-ray diffractometer (Empyrean Series 2) under CuKα radiation, at 2θ range of 15 to 90°, 0.03° step-size, was employed to identify the crystalline phases present in the as-received, delaminated, and relithiated NMC cathode materials. The relative phase weights of each sample and their lattice parameters were obtained by Rietveld refinements employing the X'Pert HighScore Plus Software. The goodness of fit parameter, $\chi^2$, was employed to qualify the performed refinements.

SEM images of all NMC cathode powders were obtained from an electronic microscope (Zeiss Evo15 ESEM) operated at 20 kV and 750 pA emission current on the Au-coated powder spread over a carbon tape substrate.

The particle size of the powder samples was analyzed using laser diffraction and dynamic image analysis techniques (PSA Microtrac, model S3500, 0.01 to 4000 micrometers measurements range).

The changes in the masses of the as-received and relithiated powders in thermogravimetric scannings and the identification of the gases evolved were followed by a thermal analyzer coupled with a mass spectrometer (TGA-MS Netzsch STA 449 F1 Jupiter Thermal Analyser). The samples were heated from 40 °C to 1000 °C under $N_2$ at a rate of 10 °C $min^{-1}$.

Elemental composition analysis of the as-received, delaminated, and relithiated samples was measured using a carbon, hydrogen, nitrogen, and sulfur (CHNS) analyzer (Thermo Scientific Flashsmart analyzer).

### Relithiated Cathode Charge Capacity

The electrochemical performance of electrodes fabricated from the relithiated NMC was evaluated by measuring the specific charge capacity in a coin-type test cell.

The electrodes of the relithiated QCR and EoL cathode material were prepared in a dry room (dew point of −50 °C) employing carbon black (Super C65) and PVDF (Solef 5130, Solvay SA, 1120 Brussels, Belgium) dissolved in 8 wt.% NMP solution. A slurry containing the relithiated QCR or EoL materials, carbon black, and PVDF was obtained by mixing them in the 90 : 5 : 5 weight ratio and homogenized in a centrifugal mixer (Thinky ARE 250, Intertronics, Oxfordshire, UK). The electrodes were prepared by coating sheet aluminum substrates (current collectors) with the slurry by a doctor blade procedure, lead to dry on a hot plate at 80 °C, then transferred to a vacuum oven at 120 °C overnight before the cell assembly.

The NMC/Al electrode and separator sheet (Celgard 2325, Charlotte, NC, USA) were cut into disks with 14.8 mm and 16.0 mm diameters, respectively. Cells were manufactured with a lithium metal counter electrode and filled with 70 μL electrolyte formed by 1.0 M $LiPF_6$ in 3EC:7EMC solvent proportions (PuriEl R&D261, Soulbrian, MI, USA).

Electrochemical tests were conducted using a Bio-Logic BCS 805 series cycler. After assembling the cells, they were held at open circuit voltage (OCV) for six hours, followed by cycling with a charge current density of 10 mA $g^{-1}$ to 4.3 V and discharge at the same current density to 2.5 V. This cycling protocol (electrode formation) was repeated twice to enhance the formation of the solid electrolyte interface (SEI) and stabilize reactions that might occur in the initial cycles of the cell.

Following the formation protocol, the cells underwent cycling with a charge and discharge current density of 30 mA $g^{-1}$. However, at the end of every twenty cycles, the discharge current density was increased to 150 mAh $g^{-1}$, and this procedure was repeated until completed one hundred cycles. The cells were charged using the CC–CV protocol and discharged in CC.

## Acknowledgements

L.E Sita thanks CAPES for his scholarships in the doctoral program and research internship at the University of Birmingham. Part of this study was financed by the Coordenação de Aperfeiçoamento de Pessoal de Nível Superior-Brasil (CAPES) – Finance Code 001. J.Scarminio thanks CNPq for the granted fellowship (DT2-310364/2022-1). The authors are grateful for the financial support from Faraday Institution, ReLiB (FIRG057), NEXTRODE (FIRG066) and CATMAT (FIRG063) projects for funding. This project has also received funding from the European Union's Horizon Europe research and innovation program under grant agreement No. 101137585, REVITALISE

## Conflict of Interests

The authors declare no conflict of interest.

## Data Availability Statement

The data that support the findings of this study are available in the supplementary material of this article.

**Keywords:** Direct recycling · Relithiation · NMC532 cathode · Production scrap · End-of-life, batteries

[1] T. Kim, W. Song, D. Y. Son, L. K. Ono, Y. Qi, *J. Mater. Chem A Mater.* **2019**, *7*, 2942.
[2] G. Harper, R. Sommerville, E. Kendrick, L. Driscoll, P. Slater, R. Stolkin, A. Walton, P. Christensen, O. Heidrich, S. Lambert, A. Abbott, K. Ryder, L. Gaines, P. Anderson, *Nature* **2019**, *575*, 75.
[3] L. A. W. Ellingsen, G. Majeau-Bettez, B. Singh, A. K. Srivastava, L. O. Valøen, A. H. Strømman, *J. Ind. Ecol.* **2014**, *18*, 113.
[4] L. Gaines, *Sustain. Mater. Technol.* **2014**, *1*, 2.
[5] D. Marchese, C. Giosuè, A. Staffolani, M. Conti, S. Orcioni, F. Soavi, M. Cavalletti, P. Stipa, *Batteries* **2024**, *10*, 27.
[6] R. P. Sheth, N. S. Ranawat, A. Chakraborty, R. P. Mishra, M. Khandelwal, *Energies (Basel)* **2023**, *16*, 3228.
[7] M. T. Islam, U. Iyer-Raniga, *Recycling* **2022**, *7*, 33.
[8] L. Gaines, Q. Dai, J. T. Vaughey, S. Gillard, *Recycling* **2021**, *6*, 2.
[9] M. Mancini, M. F. Hoffmann, J. Martin, D. Weirather-Köstner, P. Axmann, M. Wohlfahrt-Mehrens, *J. Power Sources* **2024**, *595*, 233997.
[10] T. Li, X. Z. Yuan, L. Zhang, D. Song, K. Shi, C. Bock, *Electrochem. Energy Rev.* **2020**, *3*, 43.
[11] Y. Lan, X. Li, G. Zhou, W. Yao, H. M. Cheng, Y. Tang, *Adv. Sci.* **2024**, *11*, 2304425.
[12] G. Qian, J. Wang, H. Li, Z. F. Ma, P. Pianetta, L. Li, X. Yu, Y. Liu, *Natl. Sci. Rev.* **2022**, *9*, 2.
[13] T. Li, X. Z. Yuan, L. Zhang, D. Song, K. Shi, C. Bock, *Electrochem. Energy Rev.* **2020**, *3*, 43.
[14] F. Lin, I. M. Markus, D. Nordlund, T. C. Weng, M. D. Asta, H. L. Xin, M. M. Doeff, *Nat. Commun.* **2014**, *5*, 3529.
[15] T. Rahman, T. Alharbi, *Batteries* **2024**, *10*, 220.
[16] G. Wei, Y. Liu, B. Jiao, N. Chang, M. Wu, G. Liu, X. Lin, X. F. Weng, J. Chen, L. Zhang, C. Zhu, G. Wang, P. Xu, J. Di, Q. Li, *iScience* **2023**, *26*, 107676.
[17] Y. Ji, E. E. Kpodzro, C. T. Jafvert, F. Zhao, *Clean Technol. Recycling* **2021**, *1*, 124.
[18] X. Zhang, Q. Xue, L. Li, E. Fan, F. Wu, R. Chen, *ACS Sustainable Chem. Eng.* **2016**, *4*, 7041.
[19] E. Fan, L. Li, Z. Wang, J. Lin, Y. Huang, Y. Yao, R. Chen, F. Wu, *Chem. Rev.* **2020**, *120*, 7020.
[20] A. Vanderbruggen, A. Salces, A. Ferreira, M. Rudolph, R. Serna-Guerrero, *Minerals* **2022**, *12*.
[21] A. T. Montoya, Z. Yang, E. U. Dahl, K. Z. Pupek, B. Polzin, A. Dunlop, J. T. Vaughey, *ACS Sustainable Chem. Eng.* **2022**, *10*, 13319.
[22] Y. Shi, G. Chen, F. Liu, X. Yue, Z. Chen, *ACS Energy Lett.* **2018**, *3*, 1683.
[23] A. Zorin, T. Song, D. Gastol, E. Kendrick, *Metals (Basel)* **2023**, *13*, 1276.
[24] Y. Ji, E. E. Kpodzro, C. T. Jafvert, F. Zhao, *Clean Technol. Recycling* **2021**, *1*, 124.
[25] R. Jung, M. Metzger, F. Maglia, C. Stinner, H. A. Gasteiger, *J. Electrochem. Soc.* **2017**, *164*, A1361.
[26] Y. Jung, B. Yoo, S. Park, Y. Kim, S. Son, *Metals (Basel)* **2021**, *11*, 1336.
[27] P. Liu, L. Xiao, Y. Tang, Y. Chen, L. Ye, Y. Zhu, *J. Therm. Anal. Calorim.* **2019**, *136*, 1323.
[28] M. Mancini, M. F. Hoffmann, J. Martin, D. Weirather-Köstner, P. Axmann, M. Wohlfahrt-Mehrens, *J. Power Sources* **2024**, *595*, 233997.
[29] Z. Peng, Q. Yan, K. Du, G. Hu, Z. Luo, Z. Fang, Z. Li, X. Wang, Q. Jiang, Y. Cao, *Ionics (Kiel)* **2023**, *29*, 3013.
[30] R. Sim, Z. Cui, A. Manthiram, *ACS Energy Lett.* **2023**, *8*, 5143.
[31] D. A. Ferreira, L. M. Z. Prados, D. Majuste, M. B. Mansur, *J. Power Sources* **2009**, *187*, 238.
[32] L. F. Malmonge, L. H. C. Mattoso, *Plymer* **2000**, *41*, 8387–8391.
[33] V. Gupta, X. Yu, H. Gao, C. Brooks, W. Li, Z. Chen, *Adv. Energy Mater.* **2023**, *13*, 2203093.
[34] O. Clemens, P. R. Slater, *Rev. Inorg. Chem.* **2013**, *33*, 105.
[35] M. Kobayashi, K. Tashiro, H. Tadokoro, *Molecular Vibrations Three Crystal Forms Poly(Vinylidene Fluoride)* **1976**, *8*, 2.
[36] S. P. da Silva, L. E. Sita, C. S. dos Santos, J. Scarminio, *J. Alloys Compd.* **2019**, *810*, 151933.
[37] N. Awanis Hashim, Y. Liu, K. Li, *Chem. Eng. Sci.* **2011**, *66*, 1565.
[38] M. F. Rabuni, N. M. Nik Sulaiman, M. K. Aroua, N. A. Hashim, *Ind. Eng. Chem. Res.* **2013**, *52*, 15874.
[39] J. Scarminio, A. Talleddo, A. A. Anderson, S. Passerini, F. Decker, *Electrochemica Acta* **1993**, *38*, 1637–1642.
[40] F. H. Pavoni, L. E. Sita, C. S. dos Santos, S. P. da Silva, P. R. C. da Silva, J. Scarminio, *Powder Technol.* **2018**, *326*, 78.
[41] L. Geng, J. Liu, D. L. Wood, Y. Qin, W. Lu, C. J. Jafta, Y. Bai, I. Belharouak, *ACS Appl. Energ. Mater.* **2020**, *3*, 7058.
[42] S. Jo, S. Seo, S. K. Kang, I. Na, S. Kunze, M. Song, H. San, S. P. Woo, S. H. Kim, W. B. Kim, J. Lim, *Adv. Mater.* **2024**, *36*, 2402024.
[43] P. Liu, L. Xiao, Y. Tang, Y. Chen, L. Ye, Y. Zhu, *J. Therm. Anal. Calorim.* **2019**, *136*, 1323.
[44] J. Lu, Y. Zhang, W. Huang, M. Omran, F. Zhang, L. Gao, G. Chen, *Renewable Energy* **2023**, *206*, 86.
[45] Z. Yan, A. Sattar, Z. Li, *Resour. Conserv. Recycl.* **2023**, *192*, 106937.
[46] H. Shen, H. Wang, M. Li, C. Li, Y. Zhang, Y. Li, X. Yang, X. Feng, M. Ouyang, *Electronics (Switzerland)* **2023**, *12*, 1603.
[47] R. Shunmugasundaram, R. Senthil Arumugam, J. R. Dahn, *Chem. Mater.* **2015**, *27*, 757.
[48] G. Bieker, M. Winter, P. Bieker, *Phys. Chem. Chem. Phys.* **2015**, *17*, 8670.
[49] S. H. Kang, W. S. Yoon, K. W. Nam, X. Q. Yang, D. P. Abraham, *J. Mater. Sci.* **2008**, *43*, 4701.

Manuscript received: September 21, 2024
Accepted manuscript online: September 25, 2024
Version of record online: November 7, 2024